

Mechanical probes of resonances and quasi-bound states in irregularly shaped, amplifying dielectric micro-cavities

Henning Schomerus,¹ Jan Wiersig,² and Martina Hentschel³

¹Max-Planck-Institut für Physik komplexer Systeme, Nöthnitzer Str. 38, 01187 Dresden, Germany

²Institut für theoretische Physik, Universität Bremen, Postfach 330 440, 28334 Bremen, Germany

³Department of Physics, Duke University, Box 90305, Durham, NC 27708-0305

(Dated: September 2003)

We show that the force and torque exerted by light pressure on an irregularly shaped dielectric resonator allow to detect resonant frequencies, delivering information complementary to the scattering cross-section by mechanical means. The far-field emission pattern of the associated quasi-bound states can be tested by the angular dependence of the probes at finite amplification rate.

PACS numbers: 03.65.Nk, 05.45.Mt, 42.25.-p, 42.60.Da

Waves confined in irregularly shaped geometries pose practical and theoretical challenges, as an intricate interference pattern arises from the multiple coherent scattering off the confining boundaries. This is especially true at resonant conditions, when the multiple scattering results in systematic constructive interference. Realizations of wave confinement can be found in the mesoscopic physics of electrons in quantum dots, and in microscopic dielectric systems, such as micro-optical lasers made of semiconductors [1], micro-crystals [2], or laser dye droplets [3] — systems that are promising candidates for future electronic and photonic computation and communication devices. The most direct probes of these systems are scattering experiments: Quantum dots are attached to two biased electrodes, and transmission properties are obtained from the conductance. The micro-optical systems are illuminated with a coherent light source, and the angularly resolved scattering cross-section is detected. This allows to determine resonances and, ultimately, helps to infer information about the quasi-bound states (found at complex energies or frequencies), which are the most fundamental theoretical characteristics of these open systems. The quasi-bound states can be observed as the working modes of micro-disk lasers, for which irregular shapes are favored because they permit directed emission [4].

In this paper we discuss a mechanical characterization of the resonances and the associated quasi-bound states in microscopic dielectric resonators, focusing on the practically most useful case of irregular but effectively two-dimensional geometries, and also allowing for a finite amplification rate. The probes are the force and the torque exerted by light pressure. Over the past decade, opto-mechanical tools based on light pressure have found various applications in the manipulation of microscopic objects, for which usually simple shapes have been assumed, and precision-detection of the acting forces have become commonplace [5]. We suggest to use such tools to analyze the internal wave dynamics in complicated geometries. It turns out that the mechanical response contains information which is analogous to the scattering cross-section and the delay time (the conventional probes for resonances), but is sensitive to other, complementary aspects of the quasi-

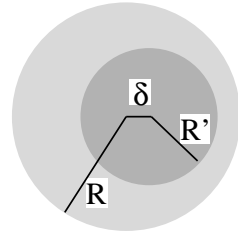


FIG. 1: The annular resonator used in the numerical investigations of this paper is composed of two circles with radii R and $R' = 0.6 R$, and eccentricity $\delta = 0.22 R$. The refractive index is $n = 1$ outside the resonator, $n = 1.8$ in the annular region between the circles, and $n = 3.3$ inside the interior circle.

bound states. Consequentially, the mechanical probes help to distinguish between different wave patterns. At finite amplification rate within the medium, they contain information on the far-field emission pattern. Our general argumentation is supported in a practical setting by numerical computations for the annularly shaped dielectric disk shown in Fig. 1, which displays a multifaceted set of wave patterns due to its non-integrable classical ray dynamics [6, 7]. We use two different numerical procedures, the wave-matching method (see e.g. Ref. [7]) and the boundary element method [8].

Resonances and quasi-bound states: For the effectively two-dimensional systems in question, we separate the two polarizations of the electromagnetic field, with either the electric field $E_z = \text{Re}[\exp(-i\omega t)\psi]$ or the magnetic field $B_z = c^{-1} \text{Re}[\exp(-i\omega t)\psi]$ polarized perpendicular to the plane. In both cases, the complex wave function ψ fulfills the two-dimensional Helmholtz equation $-\Delta\psi = n^2 k^2 \psi$, where n is the position-dependent refractive index, $k = \omega/c$ is the wave number, and c is the speed of light in vacuum. Amplification is modeled by a complex refractive index with $\text{Im } n < 0$. We choose a circular region \mathcal{A} of radius $\mathcal{R} > R$, containing the resonator, and decompose the wave function in the exterior of \mathcal{A} in the usual Hankel function basis,

$$\psi = \sum_m \left(a_m^{(\text{in})} H_m^{(2)}(kr) + a_m^{(\text{out})} H_m^{(1)}(kr) \right) e^{im\phi}, \quad (1)$$

where r and ϕ are polar coordinates. (Here and in the following, all sums run from $-\infty$ to ∞ .) The angularly resolved radiation in the far field is given by

$$I(\phi) = \frac{2}{\pi|k|} \left| \sum_m a_m^{(\text{out})} e^{im(\phi-\pi/2)} \right|^2. \quad (2)$$

Below the laser threshold, the expansion coefficients $a_m^{(\text{out})}$ of the outgoing wave are related to their incoming counterparts $a_m^{(\text{in})}$ by linear relations $a_m^{(\text{out})} = \sum_{m'} S_{mm'} a_{m'}^{(\text{in})}$, where the coefficients $S_{mm'}$ form the scattering matrix. The scattering matrix fulfills the time-reversal symmetry $S_{m,n} = S_{-n,-m}(-1)^{m+n}$, and is unitary for real k and n (for complex values, unitarity is replaced by $S^{-1}(k, n) = [S(k^*, n^*)]^\dagger$).

Quasi-bound states are found at complex values k_c of k that permit nontrivial solutions $\mathbf{a}^{(\text{out})} = \mathbf{a}_c$ of the condition of no incident radiation, $\mathbf{a}^{(\text{in})} = 0$. For the annular resonator, complex values k_c are shown in the bottom panel of Fig. 2, and some typical wave patterns are presented in the right panels of Fig. 3. For this system, the quasi-bound states occur with even and odd parity [9], and further can be divided into whispering-gallery modes at the interior interface (class W_{int}) or the exterior interface (class W_{ext}), and extended modes that we group into two classes A (inside the interior circle, these modes are of whispering-gallery character) and C (extended over the whole resonator). Close to resonance in the complex k -plane ($k \approx k_c^{(\text{even})}, k_c^{(\text{odd})}$), the scattering matrix can be approximated by

$$S \approx \frac{\mathbf{a}_c^{(\text{even})} \otimes \tilde{\mathbf{a}}_c^{(\text{even})}}{k - k_c^{(\text{even})}} + \frac{\mathbf{a}_c^{(\text{odd})} \otimes \tilde{\mathbf{a}}_c^{(\text{odd})}}{k - k_c^{(\text{odd})}} \quad (3)$$

where $\tilde{\mathbf{a}}_{c,m} = (-1)^m \mathbf{a}_{c,m}$ due to time-reversal symmetry and we accounted for the potentially quasi-degenerate partner of opposite parity (indicated by the superscripts).

In general, the quasi-bound states can be transported to real values of $k \simeq \text{Re } k_c$ when $\text{Im } n \simeq \text{Im } k_c \text{Re } n / \text{Re } k_c$, corresponding to an active, amplifying medium close to threshold [10]. Above threshold, the linear relation between $\mathbf{a}^{(\text{in})}$ and $\mathbf{a}^{(\text{out})}$ break down, but in homogeneously amplifying media the lasing modes are well approximated by the cold-resonator modes [11, 12, 13]. The far-field emission pattern $I(\phi) = I_c(\phi)$ of the laser is then given by Eq. (2), evaluated with the quasi-bound state that wins the mode competition.

The values k_c are the poles of S where this matrix is singular, and are reflected by resonances of the system at real values $k = \text{Re } k_c$. Conventional probes for resonances are obtained from the total scattering cross-section

$$\sigma = \frac{4}{k} \sum_m |a_m^{(\text{out})} - a_m^{(\text{in})}|^2, \quad (4)$$

and the weighted delay time [14]

$$\tau = 4 \text{Im} \sum_m a_m^{(\text{out})*} da_m^{(\text{out})} / d\omega. \quad (5)$$

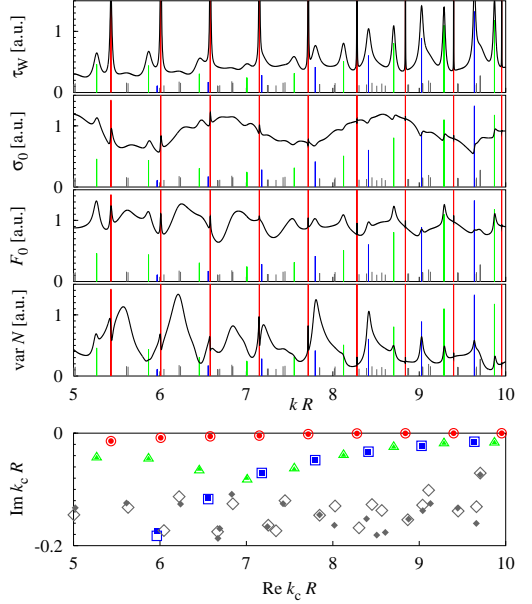


FIG. 2: (Color) The top panels show four quantities as a function of k that probe for resonances in the annular resonator: The Wigner delay time τ_W , the angle-of-incidence averaged scattering cross-section σ_0 , the angle-of-incidence averaged force in forward direction F_0 , and the variance of the torque $\text{var } N$. The lower panel shows the complex resonance wave numbers k_c of quasi-bound states, classified by their wave patterns as described in the text: W_{int} (\circ), W_{ext} (\triangle), A (\square), C (\diamond). Open symbols indicate modes of even parity, full symbols are modes of odd parity. The complex resonances are also indicated by the spikes in the top panels, located at $k = \text{Re } k_c$ with height proportional to the life time $1/(-2c \text{Im } k_c)$.

Clearly, the quantities σ and τ depend on the incoming wave, which we now specify as a plane wave coming from direction ϕ_0 [15], corresponding to $a_m^{(\text{in})} = \frac{1}{2} e^{-im(\pi/2+\phi_0)}$. Both σ and τ then provide angularly resolved information as a function of ϕ_0 . A global characterization of the system is obtained by an average over the incident radiation direction ϕ_0 , giving

$$\sigma_0 = \langle \sigma \rangle_{\phi_0} = \frac{1}{k} \sum_m (1 + \sum_{m'} |S_{mm'}|^2 - 2 \text{Re } S_{mm}), \quad (6)$$

$$\tau_W = \langle \tau \rangle_{\phi_0} = \text{Im} \text{tr } S^\dagger \frac{dS}{d\omega}, \quad (7)$$

where τ_W is known as the Wigner delay time.

Both the delay time (of predominantly theoretical virtue) and the (more practical) scattering cross-section display peaks at resonance, as is illustrated for the annular resonator in the two topmost graphs of Fig. 2. This indicates a stronger scattering of the light field and promises a marked mechanical response at resonance, which we investigate in the remainder of this paper.

Kinematics and mechanical detection of resonances: We first provide general kinematic relations for a two-dimensional resonator in a light field, which then will be used to characterize resonances and wave patterns. The mechanical forces exerted by the light field on a dielectric medium originate from

the refraction and diffraction at the dielectric interfaces — ultimately, from the deflection (and creation, at finite amplification) of the photons. The kinematics in the combined system of light field and medium can be obtained from the conservation laws of total angular and linear momentum, which equate the torque and force acting on the medium to the deficit of the angular and linear momenta carried by the electromagnetic field into and out of the circular region \mathcal{A} . (The center of this region is identified with the point of reference for the torque, and in our example is taken as the center of the exterior circle.) Note that the conservation laws also hold in an amplifying medium, due to the recoil of each created photon. The kinematic relations hence follow from integrals of Maxwell's stress tensor [16] over the boundary of \mathcal{A} . After some algebra, we find the time-averaged force and torque (per unit of thickness of the resonator) in the compact form [17]

$$F_x + iF_y = \frac{2\varepsilon_0 i}{k} \sum_m (a_m^{(\text{in})} a_{m+1}^{(\text{in})*} - a_m^{(\text{out})} a_{m+1}^{(\text{out})*}), \quad (8)$$

$$N = \frac{2\varepsilon_0}{k^2} \sum_m m \left(|a_m^{(\text{in})}|^2 - |a_m^{(\text{out})}|^2 \right). \quad (9)$$

In absence of amplification and for plane-wave illumination, it is easily seen that the direction-averaged force and torque vanish from the unitarity constraints of the scattering matrix:

$$\langle F_x + iF_y \rangle_{\phi_0} = \frac{-i\varepsilon_0}{2k} \sum_{m,m'} S_{mm'} S_{m+1,m'}^* = 0, \quad (10)$$

$$\langle N \rangle_{\phi_0} = \frac{\varepsilon_0}{2k^2} \sum_m m \left(1 - \sum_{m'} |S_{mm'}|^2 \right) = 0. \quad (11)$$

Two simple quantities that do not vanish are the mean of the force component $F_{\parallel} = F_x \cos \phi_0 + F_y \sin \phi_0$ in forward direction,

$$F_0 = \langle F_{\parallel} \rangle_{\phi_0} = \frac{\varepsilon_0}{2k} \text{Re} \sum_{m,m'} (\delta_{mm'} - S_{m'm} S_{m'+1,m+1}^*), \quad (12)$$

and the variance $\text{var } N = \langle N^2 \rangle_{\phi_0}$ of the torque,

$$\text{var } N = \frac{\varepsilon_0^2}{4k^4} \sum'_{m,m',n_1} m m' S_{mn_1}^* S_{mn_2} S_{m'n_3}^* S_{m'n_4}. \quad (13)$$

Here, the prime at the sum enforces the restriction $n_1 + n_3 = n_2 + n_4$.

Because scattering is enhanced at resonance, we expect that $\text{var } N$ and F_0 are global characteristics of the resonances comparable to σ_0 and τ_W , while N and F_{\parallel} provide angularly resolved information as a function of the incident radiation direction ϕ_0 , analogously to σ and τ . Does this promise hold true?

Figure 2 shows the global characteristics σ_0 , τ_W , $\text{var } N$, and F_0 for the annular resonator as a function of k . The plot demonstrates a clear correspondence of the resonant peaks in all four quantities. Evidently, each quantity probes a slightly

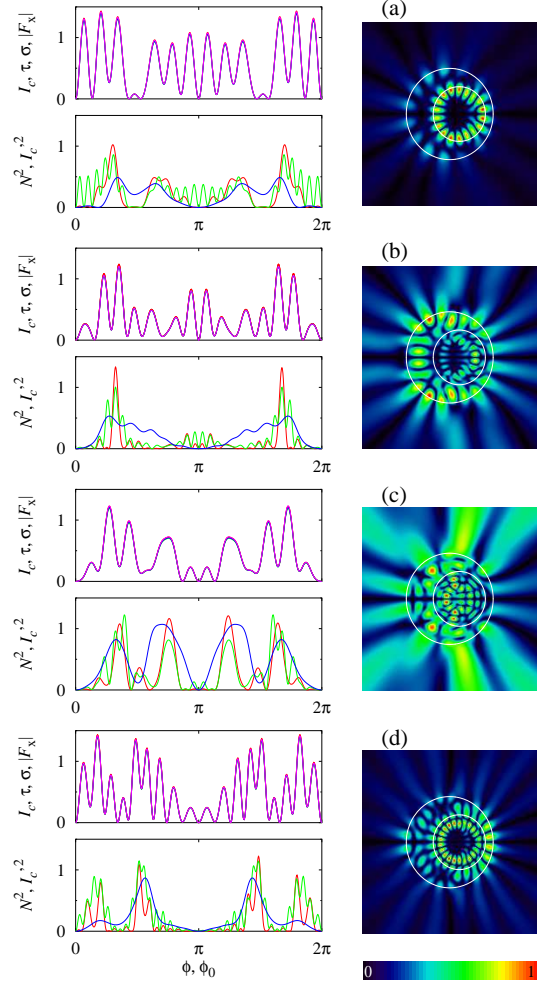


FIG. 3: (Color) The panels (a-d) show results for various combinations of k and $\text{Im } n$ tuned very close to resonance with the quasi-bound states of odd parity shown on the right, with (a) $k_c = 6.009 - i 0.008$ (class W_{int}), (b) $k_c = 7.554 - i 0.063$ (class W_{ext}), (c) $k_c = 7.847 - i 0.145$ (class C), (d) $k_c = 9.026 - i 0.022$ (class A). In the top graph of each panel, the angular dependence of the far field I (red) on the radiation direction ϕ is compared to the angular dependence on the illumination direction ϕ_0 [15] of the scattering cross-section σ (green), the weighted delay time τ (blue), and the x -component of the force, F_x (purple) — the four lines are almost indistinguishable. In the bottom graph of each panel, the (squared) torque N^2 (red) is compared to the interference term $I_c'^2$ (green), defined in Eq. (14). The blue curve is N^2 evaluated at real n . All quantities are in arbitrary units.

different aspect of the resonances, such that their relative weights are different. As usual, the delay time τ_W displays the largest peaks for the very narrow resonances associated to long-living quasi-bound states. Presently, the longest-living states are those of class W_{int} , followed by those of class W_{ext} and A, while the states of class C are hardly visible here. The scattering cross-section σ_0 displays smaller peaks (sometimes, dips) on a modulated background, and does not provide a distinctive discrimination between the different states. The

force and torque are sensitive to the wave pattern itself, and presently display a marked response especially for the quasi-bound states of class W_{ext} and A (for small k , also for class C). The torque naturally probes the anisotropy of the internal wave pattern. All quasi-bound states in Fig. 3 have rather inhomogeneous internal wave patterns, even though they do not automatically translate into very anisotropic far-field emission patterns for these rather low values of $\text{Re } k_c R$. To which extent can the far field be inferred from the angularly resolved information contained in σ , τ , N , and F ?

For real k and n , the ϕ_0 -averaged far field $I_0(\phi) = \langle I(\phi) \rangle_{\phi_0}$ is independent of ϕ . At finite amplification, however, $I_0(\phi)$ is modulated, and because of the resonant denominators in Eq. (3) it is influenced by the quasi-bound states closest in k . This is illustrated by the results shown in the left panels of Fig. 3, along with the angular dependence of σ , τ , $|F_x|$, and N on the direction of incident radiation, ϕ_0 . The values of k and $\text{Im } n$ are chosen very close to resonance with the quasi-bound states shown in the right panels. From the approximation (3) of the scattering matrix one can see that at exact resonance $\sigma(\phi_0) \sim \tau(\phi_0) \sim |F_x(\phi_0)| \sim I_c(\phi = \phi_0)$, since none of the quantities vanish for given $\mathbf{a}^{(\text{out})} = \mathbf{a}_c$ [see Eqs. (4), (5), (8)]. The correspondence of the illumination direction ϕ_0 and the radiation direction ϕ obviously relies on the time-reversal symmetry [15], which is incorporated in Eq. (3) by the relation between \mathbf{a}_c and $\tilde{\mathbf{a}}_c$. Due to the reflection symmetry of the resonator about the x axis, $|F_y| \ll |F_x|$ while $F_{\parallel} \approx \cos(\phi_0)F_x$. The symmetry also suppresses N compared to non-symmetric systems. However, N and F_y still are enhanced compared to the non-resonant situation. Let us explain this subtlety for the torque N (the discussion applies to F_y , as well). For each given quasi-bound state, $\sum_m m|a_{c,m}|^2 = 0$ because of pairwise cancellation of the terms with opposite m . Still, a non-vanishing result (of order $|k - k_c|^{-1}$) is obtained from the interference between the resonant state (with large coefficients) and the non-resonant states (with moderate coefficients). In the typical case of quasi-degeneracy, $\mathbf{a}_c^{(\text{even})}$ interferes with $\mathbf{a}_c^{(\text{odd})}$, and from Eq. (3)

$$N^2(\phi_0) \propto I_c^{(\text{even})}(\phi_0)I_c^{(\text{odd})}(\phi_0) \equiv I_c'^2(\phi_0). \quad (14)$$

This relation is indeed obeyed to good extent in the numerical computations (see Fig. 3). Even at real n , N^2 (the blue curve in the bottom graph of each panel) roughly corresponds to $I_c'^2$. In non-symmetric geometries the sum $\sum_m m|a_{c,m}|^2 \neq 0$ for a given quasi-bound state, and hence the proportionality $N \sim I_c$ (and $F_y \sim I_c$) is restored (moreover, quasi-degeneracies are then lifted, and the system more easily is tuned to resonance with individual quasi-bound states).

In summary, the force and torque exerted by light pressure on a dielectric resonator allow to detect resonances and help to characterize the wave patterns of the associated quasi-bound states. This work concentrated on the wave-optical regime, in which the wave length is not much smaller than the geometric features of the system, such that internal anisotropies

of the wave pattern cannot easily be translated into the far-field emission pattern. In the case of smaller wave lengths (large k), where such relations can be formulated in semi-classical terms, we would expect that directed emission (desired for micro-optical laser) is especially signified by the torque, which probes the anisotropy of the internal wave pattern. Moreover, isotropic modes frequently arise from a large collection of unstable ray trajectories [18], and can be described as a superposition of random waves [19]. As k is increased, more and more random-wave components become available, and hence the mechanical response is suppressed by self-averaging. Anisotropic modes are guided by just a few trajectories such that the self-averaging mechanism does not apply to them, which further enhances the selectivity of the torque for anisotropic modes.

- [1] Y. Yamamoto and R. Slusher, Phys. Today **46**, 66 (1993).
- [2] U. Vietze, O. Krauss, F. Laeri, G. Ihlein, F. Schüth, B. Limburg, and M. Abraham, Phys. Rev. Lett. **81**, 4628 (1998).
- [3] S. X. Qian, J. B. Snow, H. M. Tzeng, and R. K. Chang, Science **231**, 486 (1986).
- [4] C. Gmachl, F. Capassa, E. E. Narimanov, J. U. Nöckel, A. D. Stone, J. Faist, D. L. Sivco, and A. Y. Cho, Science **280**, 1556 (1998).
- [5] See e.g. A. Ashkin, Proc. Natl. Acad. Sci. USA **94**, 4853 (1997).
- [6] O. Bohigas, D. Boosé, R. Egydio de Carvalho, and V. Marvulle, Nucl. Phys. A **560**, 197 (1993).
- [7] M. Hentschel and K. Richter, Phys. Rev. E **66**, 056207 (2002).
- [8] J. Wiersig, J. Opt. A: Pure Appl. Opt. **5**, 53 (2003).
- [9] The splitting of the almost-degenerate pairs of whispering-gallery modes is related to the dynamical tunneling investigated in E. Doron and S. D. Frisch, Phys. Rev. Lett. **75**, 3661 (1995); G. Hackenbroich and J. U. Nöckel, Europhys. Lett. **39**, 371 (1997).
- [10] The values are slightly shifted, since there is no amplification outside the medium.
- [11] A. E. Siegmann, *Lasers* (University Science Books, Mill Valley, CA, 1986).
- [12] T. Sh. Misirpashaev and C. W. J. Beenakker, Phys. Rev. A **57**, 2041 (1998); M. Patra, Phys. Rev. A **65**, 043809 (2002).
- [13] For inhomogeneous media, see H. Cao et al., Phys. Rev. B **67**, 161101 (2003); M. Patra, e-print cond-mat/0302506 (2003); L. I. Deych, e-print cond-mat/0306538 (2003).
- [14] F. T. Smith, Phys. Rev. **118**, 349 (1960); Y. V. Fyodorov and H.-J. Sommers, J. Math. Phys. **38**, 1918 (1997); A. Z. Genack, P. Sebbah, M. Stoytchev, and B. A. van Tiggelen, Phys. Rev. Lett. **82**, 715 (1999).
- [15] Note that ϕ_0 is the direction to the light source, i.e., the incoming field actually propagates in direction $\phi_0 + \pi$. With this definition, ϕ_0 and ϕ indeed denote directions related by time-reversal symmetry.
- [16] J. D. Jackson, *Classical Electrodynamics* (John Wiley & Sons, New York, 1975).
- [17] For formulas applying to spheres, see J. P. Barton, D. R. Alexander, and S. A. Schaub, J. Appl. Phys. **66**, 4594 (1989).
- [18] M. C. Gutzwiller, *Chaos in Classical and Quantum Mechanics*, vol. 1 of *Interdisciplinary Applied Mathematics* (Springer, Berlin, 1990).
- [19] M. V. Berry, J. Phys. A **10**, 2083 (1977).